Organic & Biomolecular Chemistry

Accepted Manuscript

This article can be cited before page numbers have been issued, to do this please use: H. Wang, J. Zhao, G. Yang, F. Zhang, J. Sun and R. Lu, *Org. Biomol. Chem.*, 2018, DOI: 10.1039/C8OB00113H.

ROYAL SOCIETY OF CHEMISTRY

rsc.li/obc

View Article Online
DOI: 10.1039/C8OB00113H

Journal Name

ARTICLE

Diarylethenes-based xerogels: the fabrication of more entangled networks driven by isomerization and acidofluorochromism

Received 00th January 20xx,
Accepted 00th January 20xx

DOI: 10.1039/x0xx00000x

www.rsc.org/MaterialsC

Haoran Wang,[a] Jinyu Zhao,[a] Guojian Yang,[a] Fushuang Zhang,[a] Jingbo Sun,[a] Ran Lu*[a]

Full-conjuagted styrylbenzoxazoles and styrylbenzothiazoles of **BOAF24**, **BOACl24**, **BOACl35**, **BOABr24**, **BOABr35**, **BTAF24**, **BTACl24** and **BTABr24** without traditional gelation groups could form organogels. It was found that the introduction of chlorine atoms in 2,4-positions of phenyl group would improve the gelation abilities, and benzothiazole derivatives exhibited better gelation abilities than benzoxazoles with similar π-skeleton due to the better π-electron delocalization. Interestingly, the organogel of **BTACl24** could be destroyed into solution by UV light due to *trans-cis* isomerization, which could also induce the morphological changes of xerogels. The smooth organogel nanofibers stretched out lots of thin 'arms' to hold together or to catch other nanofibers upon UV irradiation, so more entangled networks were generated. Moreover, TFA (trifluoroacetic acid) could induce gel-sol transformation on account of the protonation of benzoxazole or benzothiazole unit, accompanied with the quenching of the emission. **BTACl24** exhibited higher performance than **BOACl24** in the detection of TFA because of its strong basicity. The decay time and the detection limit of **BTACl24** in xerogel-based film towards TFA vapor were of 0.7 s and 0.3 ppm, respectively. Therefore, the organogelation of non-traditional organogelators is powerful way to fabricate multi-stimuli-responsive soft materials, and it provided a new method to generate more entangled 3D networks through the photochemical reaction in xerogels.

Introduction

Low molecular weight organogels (LMOGs) fabricated from π-organogelators have received recent attention due to their potential applications in optoelectronic devices,[1] chemosensors,[2] field-effect transistors,[3] and so on. It is well-known that the π-gelators tend to form 1D aggregates directed by intermolecular interactions, especially π-π interactions,[4] followed by intertwine into 3D network, so that the π-gels are sensitive to external stimuli of heat, light, chemical, sound and mechanical force.[5] Compared with the traditional π-gelators, the synthesis of the non-traditional organogelator excluding the auxiliary groups of long alkyl chains, sugar, cholesterol or H-bonding units showed high atom economy.[6] To date, the design of non-traditional π-gelators is still changeling since it is difficult to balance the intermolecular interactions of full-conjugated compounds. Park et al. found that the stilbenes bearing -CN or/and -CF_3 self-assembled into nanowires driven by C-H···F and π-π interactions.[7] Fan reported a series of non-traditional π-gelators based on dendrons and dendrimers of poly(benzyl ether).[8] Würthner reported a perylenebisimide-based organogelator lacking long alkyl chains and H-bonding unit.[9] Recently, our group has synthesized a series of non-traditional π-gelators based on the derivatives of *tert*-butylcarbazole,[10] β-diketone/salicylaldimine difluoroboron complexes[11] and full-conjugated carbazolevinyl benzoxazole,[12] and found that the introduction of halogens could improve the gelation abilities.[13] In order to reveal the effect of halogen on the self-assembling of full-conjugated systems, we have synthesized new styrylbenzoxazoles bearing different kinds of halogens in different positions in benzene rings except for **BOACl4** and **BOACl24**, which have been reported in previous work (Scheme 1).[14] It was found that **BOAF4**, **BOACl4** and **BOABr4** bearing one halogen atom could not form any gel in the tested solvents. The 2,4-dihalogenstyrylbenzoxazoles of **BOAF24**, **BOACl24** and **BOABr24** showed strong gelation abilities than the corresponding 3,5-dihalogenstyrylbenzoxazoles of **BOAF35**, **BOACl35** and **BOABr35**, respectively. Accordingly, the 2,4-dihalogenstyrylbenzothiazoles **BTAF24**, **BTACl24** and **BTABr24** were prepared. Interestingly, they showed more excellent self-assembling abilities compared with styrylbenzoxazoles in similar structures. Notably, the light-induced *trans-cis* isomerization of **BTACl24** led to the gel-sol transformation and the morphologic changes of the xerogel. In detail, lots of thin 'arms' were stretched out from the smooth nanofibers, and they would hold together or caught other nanofibers. The networks were turned into a crisscross pattern. To the best of our knowledge, such phenomenon was not reported elsewhere. It should be noted that the organogel of **BTACl24** and **BOACl24** could be destroyed upon the addition of TFA, accompanied with the quenching of the emission on account

[a] Sate Key Laboratory of Supramolecular Structure and Materials, College of Chemistry, Jilin University, Changchun, P.R. China. E-mail: luran@mail.jlu.edu.cn.

†Electronic Supplementary Information (ESI) available: ^{1}H NMR and ^{13}C NMR spectra; HRMS; Photophysical data; UV-Vis absorption spectra; Fluorescent emission spectra and XRD patterns in solid states. See DOI: 10.1039/x0xx00000x

of the protonation of benzothiazole and benzoxazole moieties. **BTACl24** exhibited higher performance than **BOACl24** in the detection of TFA in solutions and in xerogels on account of its strong basicity. Although pyrene- and anthracene-based organogels are typical emissive soft materials, exhibiting enhancement of power-conversion efficiency of solar cell, circularly polarized luminescence and multi-responsive properties,[15] the self-assembling processes were assisted by traditional gelation groups. Therefore, the organogelation of non-traditional organogelators becomes a powerful way to fabricate multi-stimuli-responsive soft materials, and we provided a new method to generate more entangled 3D networks through the photochemical reaction in xerogels.

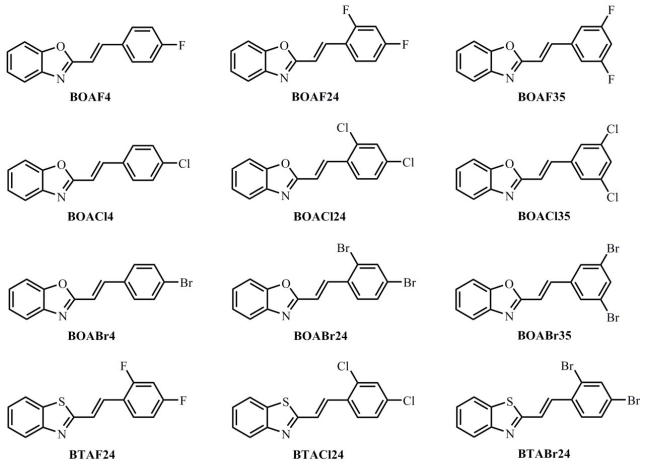

Scheme 1 Molecular structures of styrylbenzoxazole and styrylbenthiazole derivatives.

Results and discussion

Synthesis

The synthetic routes for (halogenated styryl)-benzoxazoles and (halogenated styryl)-benzothiazoles were shown in Scheme 2. They were prepared via Knoevenagel condensation reactions of 2-methylbenzoxazole/2-methylbenzothiazole with halogen-substituted benzaldehydes in THF using *t*-BuOK as catalyst. The crude products were purified by column chromatography (silica gel) using ethyl acetate/petroleum ether (v/v =1/10) as the eluent, and the yields were in the range of 42-80%. The target compounds were characterized by ^{1}H NMR, ^{13}C NMR, FT-IR and HRMS.

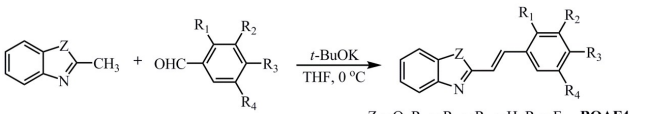

Z = O, R_1 = R_2 = R_4 = H, R_3 = F **BOAF4**
Z = O, R_1 = R_3 = F, R_2 = R_4 = H **BOAF24**
Z = O, R_1 = R_3 = H, R_2 = R_4 = F **BOAF35**
Z = O, R_1 = R_3 = H, R_2 = R_4 = Cl **BOACl35**
Z = O, R_1 = R_2 = R_4 = H, R_3 = Br **BOABr4**
Z = O, R_1 = R_3 = Br, R_2 = R_4 = H **BOABr24**
Z = O, R_1 = R_3 = H, R_2 = R_4 = Br **BOABr35**
Z = S, R_1 = R_3 = F, R_2 = R_4 = H **BTAF24**
Z = S, R_1 = R_3 = Cl, R_2 = R_4 = H **BTACl24**
Z = S, R_1 = R_3 = Br, R_2 = R_4 = H **BTABr24**

Scheme 2 Synthetic routes for styrylbenzoxazoles and styrylbenthiazoles.

Photophysical properties

The UV-vis absorption and fluorescence emission spectra of **BOACl4**, **BOACl24** and **BOACl35** in CH_2Cl_2 (1.0×10^{-5} M) were shown in Figure 1. The absorption bands of **BOACl4**, **BOACl24** and **BOACl35** appeared at 327 nm, 331 nm and 329 nm, respectively, due to π-π^* transitions. Meanwhile, the fluorescence emission bands at 402 nm, 410 nm and 404 nm were detected for **BOACl4**, **BOACl24** and **BOACl35**, respectively. It suggested that the number and position of chlorine atom in benzene ring had less effect on the electronic spectra of styrylbenzoxazole. The slight red-shifts of the absorption and emission bands for **BOACl24** compared with **BOACl4** and **BOACl35** were resulted from the conjugation effects of two chlorine atoms in 2,4-positions of benzene ring. Similarly, the UV-vis absorption and fluorescence emission bands of **BOABr24** emerged at 334 nm and 401 nm (Figure S1 and Table S1), respectively, giving slight red-shift compared with the other two bromo-substituted styrylbenzoxazole. For example, the absorption/emission bands for **BOABr4** and

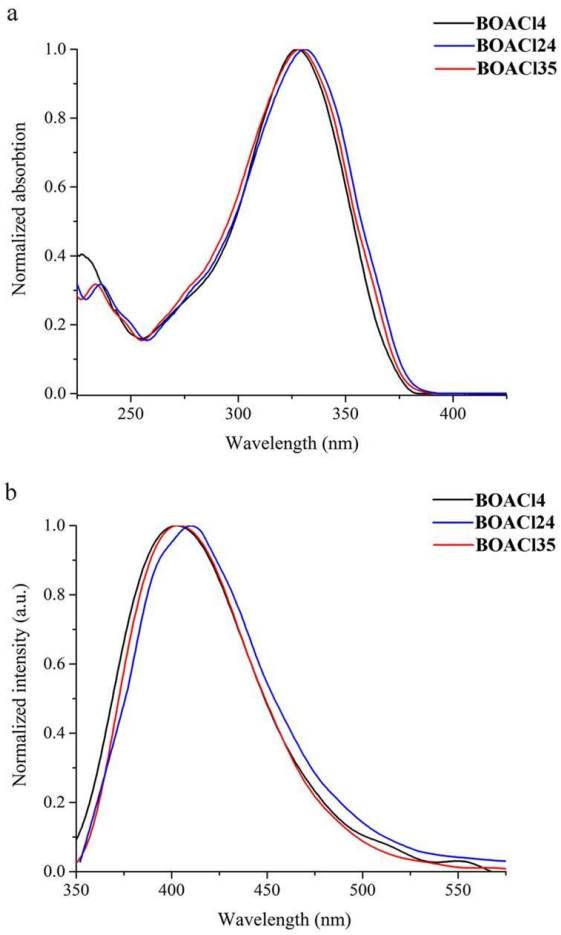

Figure 1. Normalized UV-vis absorption (a) and fluorescence emission (b, λ_{ex} = 325 nm) spectra of **BOACl4**, **BOACl24** and **BOACl35** in CH_2Cl_2.

View Article Online DOI: 10.1039/C8OB00113H

BOABr35 appeared at 328 nm/399 nm and 329 nm/400 nm, respectively. In the case of styrylbenzothiazoles, the absorption and emission bands were red-shifted compared with the styrylbenzoxazole with similar structures on account of their good π-electron delocalization. For instance, the absorption and emission of **BTABr24** emerged at 340 nm and 420 nm, respectively (Figure S2). The fluorescent quantum yields (Φ_F) of the synthesized compounds were in the range of 0.03-0.11 using quinine sulfate in 0.1 mol·L^{-1} sulfuric acid solution as the standard (Φ_F = 57%, Table S1).

Self-assembling properties

As listed in Table 1 and Table S2, the synthesized styrylbenzoxazole derivatives were soluble in CH_2Cl_2, chloroform, ethyl acetate, DMF and DMSO. **BOAF4**, **BOACl4** and **BOABr4** bearing one halogen atom could not form any organogel in the tested solvents. The dibromo-substituted styrylbenzoxazoles of **BOABr24** and **BOABr35** could form organogels in *n*-butanol with criticalgelation concentration (CGC) of 5 mg·mL^{-1} and 10 mg·mL^{-1}, respectively, besides ethanol organogel could be generated from **BOABr24**. The above phenomenon suggested that the gelation ability of **BOABr24** was stronger than **BOABr35** to some extent. In particular, the dichloro-substituted styrylbenzoxazoles exhibited relatively strong self-assembling abilities compared with dibromo-substituted styrylbenzoxazoles since the organogels could be formed from **BOACl24** and **BOACl35** in petroleum ether, cyclohexane, methanol and ethanol with CGC in the range of 2.9-6.7 mg·mL^{-1} and 5.0-10.0 mg·mL^{-1}, respectively. Likewise, the gelation ability of **BOACl24** was the strongest among the synthesized chloro-substituted styrylbenzoxazoles. It was clear that ca. 2.5 × 10^3 methanol molecules could be gelated by one **BOACl24** molecule, so **BOACl24** could be deemed as a supraorganogelator.[13] Since the gelation abilities of 2,4-dihalogen substituted styrylbenzoxazoles were better than 3,5-dihalogen substituted styrylbenzoxazoles, we synthesized 2,4-dihalogen-substituted styrylbenzothiazoles (**BTAF24**, **BTACl24** and **BTABr24**). Among them, **BTACl24** and **BTABr24** could self-assemble into organogels in petroleum ether, cyclohexane, methanol, ethanol with low CGC of 1.6-2.0 mg·mL^{-1} and 2.5-6.5 mg·mL^{-1}, respectively, and they could also be recognized as

Table 1 Gelation abilities of styrylbenzoxazole and styrylbenzothiazole derivatives in selected organic solvents.[a]

Solvent	**BOAF24**	**BOACl24**	**BOACl35**	**BOABr24**	**BOABr35**	**BTAF24**	**BTACl24**	**BTABr24**
Petroleum ether	P	G (5.0)	G (10.0)	P	P	P	G (2.0)	G (6.5)
Cyclohexane	G (20.0)	G (6.7)	G (9.6)	P	P	P	G (1.9)	G (4.0)
Methanol	P	G (2.9)	G (5.0)	P	P	G (6.7)	G (1.8)	G (2.5)
Ethanol	S	G (5.5)	G (8.8)	G (10.0)	P	G (12.5)	S (1.6)	G (3.5)
n-Butanol	S	P	P	G (5.0)	G (10.0)	P	S (10.0)	G (3.7)
Toluene	S	S	S	P	P	S	S	P
CH_2Cl_2	S	S	S	S	S	S	S	S
Chloroform	S	S	S	S	S	S	S	S
Ethyl acetate	S	S	S	S	S	S	S	S
DMF	S	S	S	S	S	S	S	S
DMSO	S	S	S	S	S	S	S	S

[a] I: insoluble; S: soluble; G: stable gel; P: precipitate. CGC: critical gelation concentration (mg·mL^{-1}).

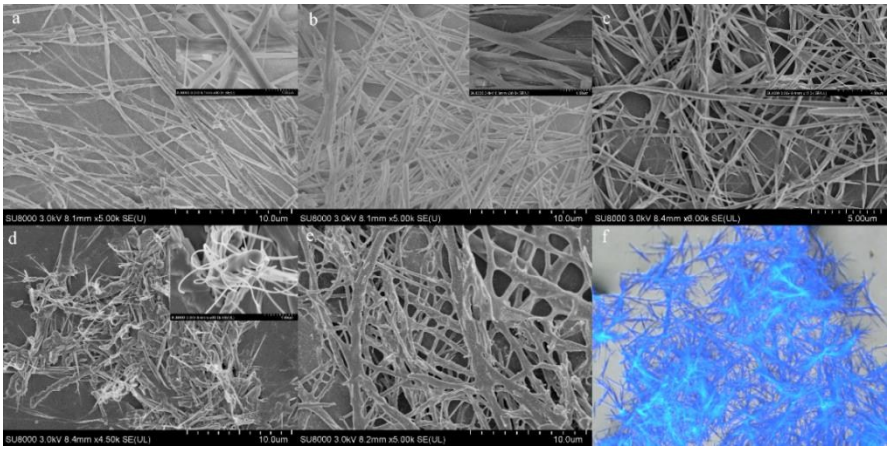

Figure 2. SEM images of the xerogels of (a) **BOACl24**, (b) **BOACl35** and (c) **BTACl24** obtained from methanol; (d) SEM image of the sample obtained by coating the solution, which was gained from methanol organogel of **BTACl24** upon UV irradiation for 60 s; (e) SEM image of the xerogel of **BTACl24** upon UV irradiation for 20 min; (f) Fluorescence microscopy image of the xerogel of **BTACl24** (λ_{ex} = 365 nm).

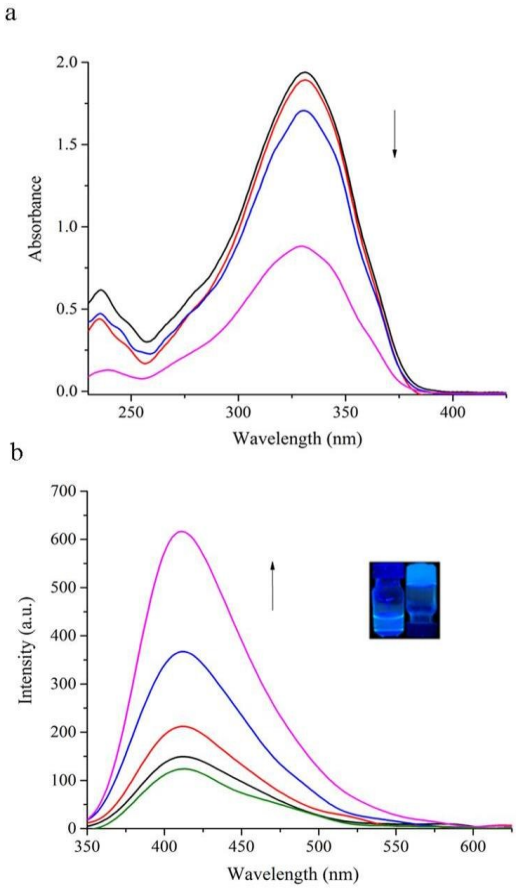

Figure 3. Time-dependent UV-vis absorption (a) and fluorescence emission (b, λ_{ex} = 320 nm) spectra of **BOACl24** upon cooling the hot solution in methanol (1.1×10^{-2} M), which was first stimulated by ultrasound to room temperature. The alternation is 15 s, and the arrows indicate the spectral changes from the sol to gel.

supraorganogelators. The styrylbenzothiazole derivatives exhibited better gelation abilities than styrylbenzoxazoles with similar molecular structures. This conclusion could be further confirmed by the fact that the organogels could be generated from **BTAF24** in methanol and ethanol with CGC of 6.7 mg·mL^{-1} and 12.5 mg·mL^{-1}, while **BOAF24** could form organogel only in cyclohexane with high CGC of 20 mg·mL^{-1}. As a result, the introduction of chlorine atoms in 2,4-position of benzene ring and the good delocalization of π-electron in styrylbenzothiazole would significantly improve the gelation abilities of non-traditional organogelators based on rigid π-conjugated systems. Moreover, the obtained organogels were stable for several months at room temperature and could be destroyed upon heating. If the hot solutions were stimulated by ultrasound again, the organogels could be reformed.

As depicted in Figure 2, SEM images of the xerogels formed from **BOACl24**, **BOACl35** and **BTACl24** in methanol illustrated that they self-assembled into lots of smooth nanofibers in diameters of 200-400 nm, which further packed into 3D networks. It should be noted that more nodes appeared in xerogel of **BTACl24** compared with **BOACl24** and **BOACl35**, so it was in accordance with the conclusion that the gelation ability of **BTACl24** was better than others.

In order to investigate the driving forces during the gel formation, the time-dependent UV-vis absorption and fluorescent emission spectra of **BOACl24** in methanol (1.1×10^{-2} M) upon cooling the hot solution, which was first stimulated by ultrasound, to room temperature were measured. As depicted in Figure 3, during the gelation process the intensity of the absorption at 331 nm decreased gradually and no spectral shift was detected. Meanwhile, the emission at 410 nm was intensified obviously, accompanied with a slight red-shift. In the organogel, the emission band emerged at 415 nm. It suggestedthat the π-π interaction had an effect on the formation of organogel.

To estimate the molecular packing mode in gel state, the XRD pattern of the xerogel of **BOACl24** obtained from methanol was given in Figure S3, and exhibited several strong and sharp diffraction peaks. In our previous work, we determined the single crystal structure of **BOACl24** (CCDC 1526199),[14] and found that most of the diffraction peaks in the simulated XRD pattern based on single crystal structure were similar to those in xerogel. Therefore, we deemed that the molecular packing modes were similar in xerogel and in single crystal. As a result, **BOACl24** might adopt a parallel layered structure in gel phase, in which *H*-aggregates were formed. The distance between two adjacent molecular planes was 3.482 Å in single crystal and a similar diffraction peak corresponding to a *d*-spacing of 0.37 nm emerged in xerogel, meaning the occurrence of π-π interactions. Moreover, we observed the distances of C-H···Cl (3.165 Å, 3.178 Å, 3.009 Å, 3.250 Å), C-H···O (2.654 Å, 3.119 Å) and C-H···N (2.811 Å, 2.792 Å, 3.648 Å) in single crystal of **BOACl24**. It was deduced that the H-bondings of C-H···Cl, C-H···O and C-H···N might be also the driving forces to direct the organogelation of **BOACl24**. It further suggested that the introduction of halogens would improve the gelation abilities. Similarly, during the organogelation of **BTACl24**, the absorption at 338 nm decreased gradually. Meanwhile, the emission intensity at 418 nm was red-shifted to 425 nm and its intensity was enhanced (Figure S4). Therefore, π-aggregates were formed from **BTACl24** in the organogel.

Additionally, the single crystal structure of **BOACl4** (CCDC 1526206) could provide some information why it could not form organogel.[14] The molecules adopted an anti-parallel layered structure, and the distance between two adjacent molecular planes was 3.653 Å, so the π-π interactions between molecules **BOACl4** were weaker than those between molecules **BOACl24** in single crystals. The distances of C-H···O (2.809 Å, 3.588 Å, 3.631 Å) and C-H···N (2.967 Å, 3.134 Å, 3.534 Å) also illustrated that the H-bondings were weaker in single crystal of **BOACl4** than those in **BOACl24**. Therefore, **BOACl4** could not form organogel was originated from the weak intermolecular interactions.

Light responsive behaviors of the organogel and xerogel

In our previous work, we have found that the nanofibers generated from **BOACl24** in organogel could curl under UV light, which was driven by light-induced [2+2] cycloaddition.[14] Therefore, we intended to investigate the light responsive

properties of the gained organogels. Although no visible macroscopic photomechanic effect was detected for the organogels of **BOACl35**, **BOABr24**, **BOABr35**, **BTACl24** and **BTABr24**, we found the organogels were destroyed into solutions upon UV irradiation, accompanied with the rapid disappearance of the nanofibers. As shown in Figure 4 and Videos S1-S2 (Supporting Information), when 365 nm light was employed to irradiate the middle part of methanol organogel of **BTACl24** in a tube from the left side, the irradiated part of the gel became transparent. After irradiation for 80 s, the tube was rotated 180° and further irradiated from left side by UV light. The middle part in gel was changed into solution absolutely when the irradiation time was prolonged to 160 s. Even if the tube was shaken slightly or was turned upside down, the rest part of gel was intact and the solution was locked in the middle. After it was placed at room temperature for 40 d, both the part of gel and the part of solution were still maintained at the original states. It further proved that the organogel was very stable. In addition, the changes of the nanofibers in methanol organogel of **BTACl24** induced by UV light was observed under microscope (Video S3 in Supporting Information), and they disappeared quickly when 365 nm light was turned on.

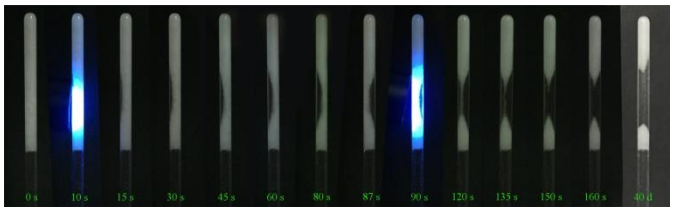

Figure 4. The gel-sol transformation of the organogel of **BTACl24** in methanol upon irradiated by 365 nm light for different time, and the tube was rotated 180° after 80 s.

To obtain the insight into the light-induced gel-sol transformation, the absorption and emission spectral changes of the methanol organogel of **BTACl24** upon exposure to 365 nm light for 1 s were studied (Figure S5a-b). The absorption band of **BTACl24** in methanol organogel was located at 338 nm, and it was blue-shifted to 301 nm after irradiated by UV light, accompanied with the significant decrease of the absorption intensity. It was clear that the light-induced gel-sol transformation was not the reverse process of organogelation. As mentioned above, the gel formation of **BTACl24** led to the decrease instead of increase of the absorption intensity at 338 nm, and no spectral shift was detected (Figure S4). Therefore, we deduced that the reason for the destruction of organogel of **BTACl24** induced by UV light was different from gel-sol transformation stimulated by heating. Accordingly, the UV-vis absorption of **BTACl24** in solution, which was gained from the organogel by heating was shown in Figure S5c. It was clear that the absorption intensity at 338 nm was significantly enhanced upon the formation of the solution from gel phase by heating. Therefore, we deemed that photochemical reaction might take place when the organogel **BTACl24** was exposed to UV light. The fluorescent emission spectra also exhibited different responsive behaviors in the course of gel-sol transformation via the treatment of heat and light. The fluorescence emission band at 425 nm for **BTACl24** in organogel was blue-shifted to 416 nm in solution gained via heating, and the intensity was declined 40%. However, the emission intensity at 425 nm for **BTACl24** in solution obtained from organogel induced by UV light was decreased to a quarter of that in organogel, and blue-shifted to 407 nm with a newly emerged shoulder at 388 nm. Thus, new species might be afforded from **BTACl24** via photochemical reaction.

Consequently, ^{1}H NMR spectra of **BTACl24** in methanol-d_4 upon UV irradiation for different time were first measured (Figure S6), and we found obvious changes in chemical shifts and the shapes of the peaks with prolonging UV irradiation. However, it was difficult to figure out the changes of the signals for H atoms, so ^{1}H NMR spectra of **BTACl24** in DMSO-d_6 upon UV irradiation were given in Figure 5. We found that the chemical shifts for H1 and H2 in **BTACl24** appeared at 7.87 ppm and 7.76 ppm, respectively, before UV irradiation, and the coupling constant was 16.0 Hz, suggesting *trans*-form of carbon-carbon double bond. After UV irradiated for 15 s, their integral values were decreased. Meanwhile, new peaks at 7.97 ppm and 7.90 ppm with coupling constant of 8.0 Hz emerged, and could be assigned to H4 and H3, respectively, in *cis*-form **BTACl24**. After irradiated for 80 s, the signals of H1 and H2 disappeared completely. We inferred that *trans-cis* isomerization of **BTACl24** took place upon exposure under UV light, which led to the gel-sol transformation of **BTACl24**.

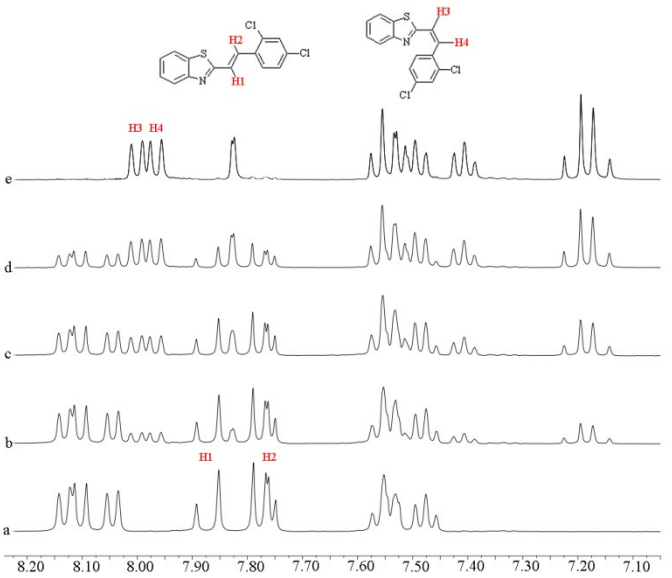

Figure 5. ^{1}H NMR spectra of **BTACl24** before (a) and after irradiated by 365 nm for 0 s (a), 15 s (b) 30 s (c) 45 s (d) and 80 s (e) in DMSO-d_6.

On the other hand, we examined the morphological changes of the aggregates in wet organogel and in the xerogel upon the exposure under UV light. Firstly, the sample was prepared by dropping the solution, which was gained via UV irradiation of the organogel **BTACl24** for 60 s, on silicon wafer. From Figure 2d, the aggregates in different shapes, including clews formed from fibrils, short nanofibers, rugged rods, small blocks and

DOI: 10.1039/C8OB00113H

blobs, were observed. It indicated that the light-induced *trans-cis* isomerization of **BTACl24** could lead to the disassembly of some organogel nanofibers and the destruction of 3D networks. Interestingly, many thin fibrils with diameter of ca. 50 nm were spit out from the thick fibers (Inset in Figure 2d). The reason might be that the strains were yielded and accumulated on the nanofibers during the light-induced isomerization process. In order to release the strain, more thin fibrils escaped from the thick fibers. Hence, we deduced that UV light might result into the morphological change of the xerogel. As anticipated, after the xerogel **BTACl24** was irradiated by 365 nm light for 20 min, the original smooth nanofibers stretched out lots of thin 'arms'. Some 'arms' from neighboring nanofibers might hold together, and some 'arms' would stretch to another nanofibers and catch them. As a result, the networks became in a crisscross pattern (Figure 2e). What's more, a lot of blotches emerged on the surface of thick nanofibers, and they were deemed to be the growing points for the 'arms' so as to release the accumlated strains. It illustrated that the photochemical reactions of gelators in xerogels might become a new strategy for the fabrication more entangled supramolecular networks, which has not been reported elsewhere.

Sensory properties towards acids in organogels and in xerogel-based films

Because benzoxazole is a weak base, we intended to investigate the sensory properties of styrylbenzoxazole towards acids. Herein, **BOACl24** is first selected as a fluorescent probe on account of its good gelation ability and intense emission in organogel and in xerogel. As shown in Figure S7, the methanol organogel of **BOACl24** emitted strong blue fluorescence centered at 415 nm. Upon the addition of 0.5 equiv. of TFA, the intensity of the emission for **BOACl24** was declined and blue-shifted to 410 nm. When 1.0 equiv. of TFA was added, the organogel was destroyed and the formed solution exhibited a weak emission at ca. 400 nm. The emission was further decreased with increasing the amount of TFA. The solution of **BOACl24** was almost non-emissive when 2.0 equiv. of TFA was added. Therefore, the organogel could be used as sensory material to detect acid by the naked eye.

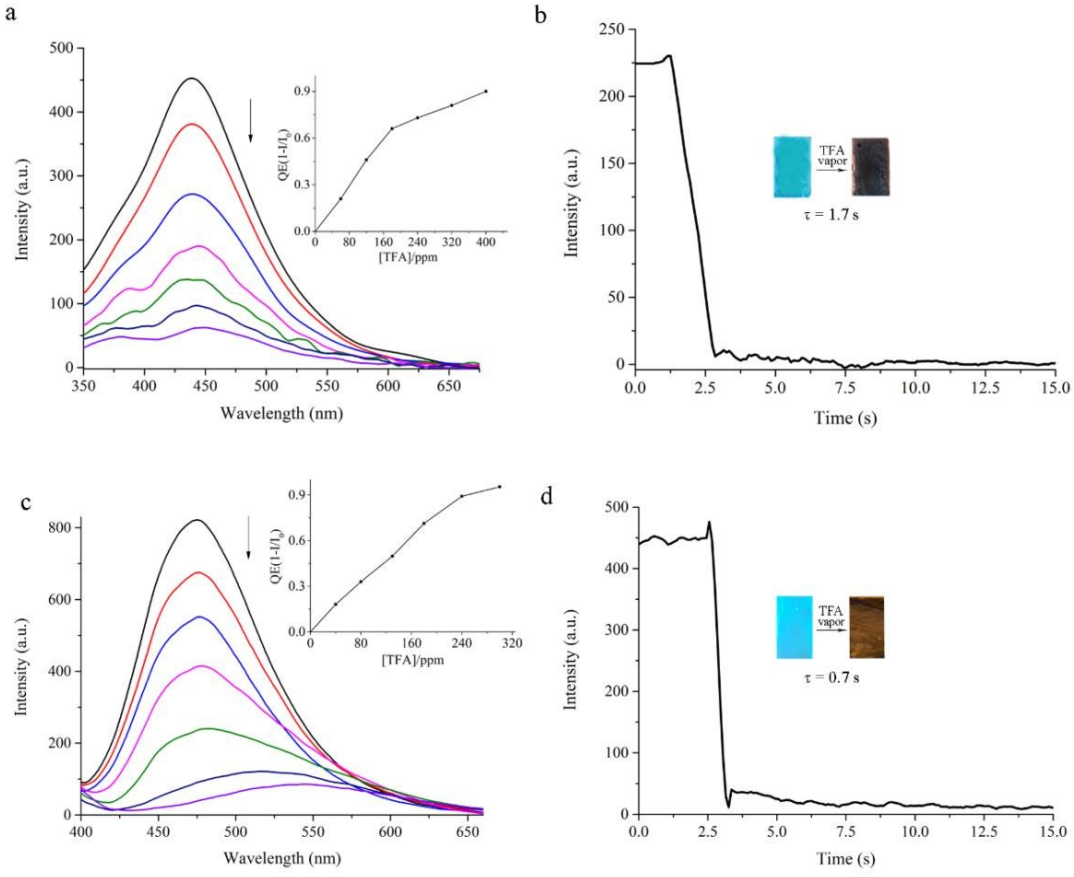

Figure 6. (a) Fluorescence emission spectra of **BOACl24** in xerogel-based film upon exposure to different amounts of TFA vapor (0-400 ppm, λ_{ex} = 320 nm). Inset: The concentration-dependent fluorescence quenching efficiencies of the film upon exposure to different amounts of TFA vapor for 2 s. (b) Time-course of the fluorescence quenching of **BOACl24** in xerogel-based film upon exposure to TFA vapor at 1000 ppm, and the intensity was monitored at 435 nm. (c) Fluorescence emission spectra of **BTACl24** in xerogel-based film upon exposure to different amounts of TFA (0-300 ppm, λ_{ex} = 330 nm). Inset: The concentration-dependent fluorescence quenching efficiencies of the film upon exposure to different amounts of TFA vapor for 2 s. (d) Time-course of the fluorescence quenching of **BTACl24** in xerogel-based film upon exposure to TFA vapor at 1000 ppm, and the intensity was monitored at 474 nm.

View Article Online
DOI: 10.1039/C8OB00113H

Journal Name

ARTICLE

It is well-known that the luminescent nanofibers-based films usually show sensitive response to analysts due to the high specific surface area as well as efficient exciton migration in 1D nanostructures.[16] Therefore, the fluorescent sensory properties of the xerogel-based film formed from **BOACl24** via organogelation were investigated. As shown in Figure 6a, the emission at 435 nm for **BOACl24** in the xerogel-based film decreased obviously upon exposed to TFA vapor. When the concentration of TFA vapor was 400 ppm, the quenching efficiency reached 90%. We found a linear relationship between the quenching efficiency and the concentration of TFA, and the detection limit was estimated to be 0.5 ppm. When the nanofibers-based film was exposed to saturated TFA vapor, the response time of the film was as short as 1.7 s. As a result, such xerogel-based film could detect TFA vapor quantitatively, sensitively and rapidly. Similarly, the xerogel-based film of **BTACl24** also exhibited excellent fluorescent sensory properties in the detection of TFA. As shown in Figure 6c, the emission at 474 nm for **BTACl24** in the xerogel-based film decreased obviously upon exposed to TFA vapor. When the concentration of TFA vapor was 300 ppm, the quenching efficiency reached 95%. Meanwhile, the detection limit and the decay time of the xerogel-based film of **BTACl24** towards TFA vapor were estimated to be 0.3 ppm and 0.7 s, respectively. Thus, **BTACl24** showed high performance in sensing TFA in xerogel-based film compared with **BOACl24**.

In order to reveal the fluorescent sensory mechanism and the differences in sensory properties of **BOACl24** and **BOACl24** towards TFA in xerogels, the electronic spectral titration experimental was performed in CH_2Cl_2. As shown in Figure S8a, the absorption band at 320 nm for **BOACl24** decreased gradually and the absorption in the range of 340-420 nm was intensified with increasing the amount of TFA. When 10 equiv. of TFA was added, new absorption at 355 nm appeared and its intensity was increased with further increasing the amount of TFA. The emergence of an isometric point at 330 nm meant the formation of new species, and we deemed the benzoxazole unit might be protonated by TFA. Meanwhile, the fluorescence emission band at 410 nm for **BOACl24** decreased gradually with increasing the amount of TFA, and the strong blue fluorescence could be quenched completely when 500 equiv. of TFA was added (Figure S8b). Therefore, the emission quenching of **BOACl24** induced by TFA in solution, organogel state and in xerogel was due to the formation of protonated **BOACl24**. On account of the increased electron-withdrawing ability of protonated benzoxazole, the intramolecular electron transfer would undergo to quench the emission. **BTACl24** gave similar fluorescence quenching behaviors towards TFA in CH_2Cl_2 (Figure S9b). Besides, in absorption titration process of **BTACl24** towards TFA, two isometric points at 270 nm and 370 nm emerged, meaning the formation of new species. Hence, we deemed that the benzothiazole might also be protonated by TFA, which was the reason for the fluorescent quenching.[17] Meanwhile, we employed an online calculation method (http://supramolecular.org/) created by P. Thordarson to calculate the binding constant (K_a).[18a] Since benzoxazole or benzothiazole (the host, H) has only one binding site with TFA (the guest, G), the fitter of UV 1:1 system was selected in the calculation. Based on the plot of the absorption of **BOACl24** at 310 nm, 315 nm and 320 nm *versus* $[G]_0/[H]_0$ in CH_2Cl_2 (Figure S8c), the k_a for **BOACl24** with TFA was estimated to be $(4.47 \pm 0.19) \times 10^4$ M^{-1}. The k_a for **BTACl24** with TFA was $(2.31 \pm 0.11) \times 10^5$ M^{-1} according to Figure S9c. It indicated that the basicity of **BTACl24** was stronger than **BOACl24**. Moreover, the fluorescence quenching data for **BOACl24** and **BTACl24** towards TFA were analyzed using the Stern-Volmer equation,[18]

$$F_0/F = 1 + K_{sv}[Q]$$

where F_0 is the initial emission intensity of probe prior to the addition of the quencher, F is the emission intensity at given concentration of the quexncher [Q], and K_{sv} is the Stern-Volmer constant. The calculated K_{sv} values for **BOACl24** and **BTACl24** towards TFA were 9278 M^{-1} and 34325 M^{-1}, respectively (Figure S8d and S9d). It suggested that **BTACl24** exhibited stronger affinity with TFA than **BOACl24**, which was consistent with the conclusion made from the online calculation. Moreover, the detection limits (LOD = $3\sigma/K_{sv}$) for **BOACl24** and **BTACl24** towards TFA were measured to be 3.2×10^{-7} mol/L and 8.7×10^{-8} mol/L, respectively. Apparently, compared with **BOACl24**, **BTACl24** could sense TFA more sensitively in CH_2Cl_2 and in xerogel on account of the strong interaction with TFA.

Conclusions

In summary, new full-conjugated non-traditional π-gelators based on styrylbenzoxazoles and styrylbenzothiazoles have been synthesized. It was found that the introduction of chlorine atoms at 2,4-position of benzene ring as well as the existence of benzothiazole with better π-electron delocalization would enhance the gelation abilities. 3D networks consisting lots of smooth nanofibers could be fabricated via organogelation process, and π-π interactions were the main driving forces for the gel formation. Interestingly, the organogel of **BTACl24** coule be destroyed into solution upon UV irradiation because of the *trans-cis* isomerization, which could further lead to the morphological change of xerogel. The smooth nanofibers stretched out lots of thin 'arms'. Some 'arms' would hold together, and some 'arms'

would catch other nanofibers. It should be noted **BOACl24** exhibited strong fluorescence in wet organogel and in xerogel, which could be quenched by TFA. In particular, the decay time and the detection limit of **BOACl24** in xerogel-based film towards TFA vapor were of 1.7 s and of 0.5 ppm, respectively, and they were decreased to 0.7 s and 0.3 ppm, respectively, for the xerogel-based film of **BTACl24** due to its strong basicity. Therefore, the organogelation of non-traditional organogelators is a powerful way to fabricate multi-stimuli-responsive soft materials and we provided a new method to fabricate more entangled supramolecular networks via photochemical reactions of π-gelators in xerogels.

Experimental section

Measurement and characterization

^{1}H NMR and ^{13}C NMR spectra were recorded with a Mercury plus instrument at 400 MHz and 101 MHz using $CDCl_3$ and DMSO-d_6 as the solvents. Mass spectra were measured with a gas chromatograph mass spectrometer GCMS-QP2010. FT-IR spectra were obtained with a Nicolet-360 FT-IR spectrometer by the incorporation of samples into KBr disks. The UV-vis absorption spectra were obtained using a Mapada UV-1800pc spectrophotometer. Fluorescence emission spectra were taken on a Cary Eclipse Fluorescence Spectrophotometer. Fluorescence microscopy images were taken on Olympus Reected Fluorescence System BX51. Scanning electron microscopy (SEM) measurements were performed on JEOL JSM-6700F (operating at 5 kV). The samples for SEM measurements were prepared by casting the organogels on silicon wafers and dried at room temperature, followed by coating with gold. X-ray diffraction pattern was obtained on Empyrean XRD equipped with graphite monochromatized Cu-Kα radiation (λ = 1.5418 Å), employing a scanning rate of 0.00267 °·s^{-1} in the 2θ range of 2 ° to 40 °. The sample for XRD measurement was prepared by casting the organogel on silicon wafer and dried at room temperature.

Preparation of organogels

The hot solutions in selected organic solvents were obtained by heating. After suffered sonification until the solutions became translucent, they were aged at room temperature for 1 min, and the organogels were formed.

Synthesis

THF was dried over sodium and benzophenone. CH_2Cl_2 was dried over calcium hydride. Water was purified with the Millipore system before used. The other chemicals and reagents were used as received without further purification.

(E)-2-(4-fluorostyryl)benzo[d]oxazole (BOAF4)

t-BuOK (0.78 g, 7.0mmol) was added into dry THF (10 mL) and stirred for 10 min at 0 °C. Then, 2-methylbenzoxazole (0.38 mL, 3.2 mmol) was added dropwise and the mixture was stirred at 0 °C for another 10 min. After that, the solution of 4-fluorobenzaldehyde (0.40 g, 3.2 mmol) in THF was added dropwise into the above solution at 0 °C. After stirred for 2 h at 0 °C, the mixture was poured into water (200 mL) and light yellow solid was collected by filtration. The crude product was purified by column chromatography (silica gel) using ethyl acetate/petroleum ether (v/v =1/10) as the eluent. Flocculus-like white solid of **BOAF4** (0.58 g) was obtained in a yield of 76%. Mp: 112.0-113.0°C. ^{1}H NMR (400 MHz, DMSO-d_6) δ (ppm): 7.94-7.88 (t, 2H), 7.84 (d, *J* = 16.4 Hz, 1H), 7.74 (t, *J* = 8.3 Hz, 2H), 7.40 (p, *J* = 7.3 Hz, 2H), 7.31 (dd, *J* = 14.9 Hz, *J* = 6.0 Hz, 3H) (Figure S10). ^{13}C NMR (101 MHz, DMSO-d_6) δ (ppm): 162.81 (s), 150.25 (s), 142.17 (s), 138.76 (s), 132.01 (d, *J* = 3.1 Hz), 130.66 (d, *J* = 8.5 Hz), 125.97 (s), 125.21 (s), 120.07 (s), 116.52 (s), 116.30 (s), 114.17 (s), 111.03 (s) (Figure S11). HRMS, m/z: calc.: 240.0819, found: 240.0826 (Figure S12). FT-IR (KBr, cm^{-1}): 1602, 1385, 1138, 1068, 992, 953, 862, 819, 539, 513.

(E)-2-(2,4-difluorostyryl)benzo[d]oxazole (BOAF24)

By following the synthetic procedure for compound **BOAF4**, **BOAF24** was synthesized from 2-methylbenzoxazole (0.38 mL, 3.2 mmol), 2,4-difluorobenzaldehyde (0.45 g, 3.2 mmol) and *t*-BuOK (0.78 g, 7.0mmol). The crude product was purified by column chromatography (silica gel) using ethyl acetate/petroleum ether (v/v = 1/10) as the eluent. Flocculus-like white solid of **BOAF24** (0.56 g) was obtained in a yield of 68%. Mp: 102.0-103.0 °C. ^{1}H NMR (400 MHz, DMSO-d_6) δ (ppm): 8.10 (dd, *J* = 15.8 Hz, *J* = 8.0 Hz, 1H), 7.82 (d, *J* = 16.6 Hz, 1H),7.78-7.75 (m, *J* = 5.7 Hz, 2H), 7.45-7.36 (m, 4H), 7.23 (t, *J* = 8.6 Hz, 1H) (Figure S13). ^{13}C NMR (101 MHz, DMSO-d$_6$) δ (ppm): 162.40 (s), 150.30 (s), 142.06 (s), 131.02-130.30 (m), 126.22 (s), 125.32 (s), 120.23 (s), 116.51 (s), 113.13 (s), 112.91 (s), 111.19 (s), 105.11 (s) (Figure S14). HRMS, m/z: calc.: 258.0725, found: 258.0729 (Figure S15). FT-IR (KBr, cm^{-1}): 1605, 1385, 1274, 1139, 1091, 967, 846, 741, 546.

(E)-2-(3,5-difluorostyryl)benzo[d]oxazole (BOAF35)

By following the synthetic procedure for compound **BOAF4, BOAF35** was synthesized from 2-methylbenzoxazole (0.38 mL, 3.2 mmol), 3,5-difluorobenzaldehyde (0.45 g, 3.2 mmol) and *t*-BuOK (0.78 g, 7.0mmol). The crude product was purified by column chromatography (silica gel) using ethyl acetate/petroleum ether (v/v = 1/10) as the eluent. Flocculus-like white solid of **BOAF35** (0.59 g) was obtained in a yield of 72%. Mp: 143.0-144.0°C. ^{1}H NMR (400 MHz, DMSO-d_6) δ (ppm): 7.82 (d, *J* = 16.4 Hz, 1H), 7.76 (ddd, *J* = 12.6, *J* = 7.3 Hz, *J* = 1.6 Hz, 2H), 7.65 (dd, *J* = 8.8 Hz, *J* = 2.0 Hz, 2H), 7.52 (d, *J* = 16.4 Hz, 1H), 7.47-7.39 (m, 2H), 7.30 (tt, *J* = 9.2, 2.3 Hz, 1H) (Figure S16). ^{13}C NMR (101 MHz, DMSO-d_6) δ (ppm): 162.23 (s), 150.30 (s), 142.07 (s), 139.13 (s), 137.49 (s), 126.36 (s), 125.36 (s), 120.32 (s), 117.27 (s), 111.51 (s), 111.25 (s), 111.15 (s), 105.35 (s) (Figure S17). HRMS, m/z: calc.: 258.0725, found: 258.0731 (Figure S18). FT-IR (KBr, cm^{-1}): 1594, 1385, 1165, 1072, 948, 859, 549, 518.

(E)-2-(3,5-dichlorostyryl)benzo[d]oxazole (BOACl35)

By following the synthetic procedure for compound **BOAF4**, **BOACl35** was synthesized from 2-methylbenzoxazole (0.38 mL, 3.2 mmol), 3,5-dichlorobenzaldehyde (0.56 g, 3.2 mmol) and *t*-

View Article Online DOI: 10.1039/C8OB00117H

BuOK (0.78 g, 7.0mmol). The crude product was purified by column chromatography (silica gel) using ethyl acetate/petroleum ether (v/v = 1/10) as the eluent. Flocculus-like white solid of **BOACl35** (0.63 g) was obtained in a yield of 68%. Mp: 144.0-145.0°C. ^{1}H NMR (400 MHz, DMSO-d_6) δ (ppm): 7.97 (d, *J* = 1.7 Hz, 2H), 7.79 (dd, *J* = 14.0, *J* = 8.8 Hz, 2H), 7.75 (d, *J* = 7.4 Hz, 1H), 7.64 (t, *J* = 1.7 Hz, 1H), 7.56 (d, *J* = 16.4 Hz, 1H), 7.44 (qd, *J* = 7.4 Hz, *J* =3.8 Hz, 2H) (Figure S19). ^{13}C NMR (101 MHz, DMSO-d_6) δ (ppm): 162.25 (s), 150.31 (s), 142.08 (s), 139.10 (s), 136.97 (s), 135.13 (s), 129.23 (s), 126.88 (s), 126.39 (s), 125.39 (s), 120.35 (s), 117.52 (s), 111.18 (s). (Figure S20). HRMS, m/z: calc.: 290.0134, found: 290.0132 (Figure S21). FT-IR (KBr, cm^{-1}): 1584, 1559, 1451, 1245, 964, 928, 837, 799, 737, 662.

(E)-2-(4-bromostyryl)benzo[d]oxazole (BOABr4)

By following the synthetic procedure for compound **BOAF4, BOABr4** was synthesized from 2-methylbenzoxazole (0.38 mL, 3.2 mmol), 4-bromobenzaldehyde (0.59 g, 3.2 mmol) and *t*-BuOK (0.78 g, 7.0mmol). The crude product was purified by column chromatography (silica gel) using ethyl acetate/petroleum ether (v/v = 1/10) as the eluent. Flocculus-like white solid of **BOABr4** (0.69 g) was obtained in a yield of 72%. Mp: 152.0-153.0 °C. ^{1}H NMR (400 MHz, DMSO-d_6) δ (ppm): 7.80 (dd, *J* = 12.0 Hz, *J* = 10.1 Hz, 3H), 7.74 (dd, *J* = 11.7 Hz, *J* = 8.4 Hz, 2H), 7.65 (d, *J* = 8.3 Hz, 2H), 7.45-7.37 (m, 3H) (Figure S22). ^{13}C NMR (101 MHz, DMSO-d_6) δ (ppm): 162.66 (s), 150.27 (s), 142.15 (s), 138.65 (s), 134.63 (s), 132.36 (s), 130.33 (s), 126.11 (s), 125.28 (s), 123.66 (s), 120.16 (s), 115.15 (s), 111.09 (s) (Figure S23). HRMS, m/z: calc.: 300.0019, found: 300.0017 (Figure S24). FT-IR (KBr, cm^{-1}): 1602, 1385, 1138, 1068, 992, 953, 862, 819, 617, 539, 513.

(E)-2-(2,4-dibromostyryl)benzo[d]oxazole (BOABr24)

By following the synthetic procedure for compound **BOAF4, BOABr24** was synthesized from 2-methylbenzoxazole (0.38 mL, 3.2 mmol), 2,4-dibromobenzaldehyde (0.84 g, 3.2 mmol) and *t*-BuOK (0.78 g, 7.0mmol). The crude product was purified by column chromatography (silica gel) using ethyl acetate/petroleum ether (v/v = 1/10) as the eluent. Flocculus-like white solid of **BOABr24** (0.66 g) was obtained in a yield of 57%. Mp: 155.0-156.0 °C. ^{1}H NMR (400 MHz, DMSO-d_6) δ (ppm): 8.05 (d, *J* = 8.5 Hz, 1H), 8.03 (d, *J* = 1.9 Hz, 1H), 7.96 (d, *J* = 16.3 Hz, 1H), 7.79 (dd, *J* = 7.6 Hz, *J* = 1.4 Hz, 2H), 7.70 (dd, *J* = 8.5 Hz, *J* = 1.8 Hz, 1H), 7.49-7.39 (m, 3H) (Figure S25). ^{13}C NMR (101 MHz, DMSO-d_6) δ (ppm): 162.12 (s), 142.03 (s), 135.96 (s), 135.60 (s), 133.85 (s), 131.81 (s), 129.81 (s), 126.44 (s), 125.43 (s), 124.02 (s), 120.37 (s), 117.99 (s), 111.33 (s) (Figure S26). HRMS, m/z: calc.: 379.9104, found: 319.9109 (Figure S27). FT-IR (KBr, cm^{-1}): 1602, 1385, 1267, 1138, 1068, 993, 952, 862, 541, 517.

(E)-2-(3,5-dibromostyryl)benzo[d]oxazole (BOABr35)

By following the synthetic procedure for compound **BOAF4**, **BOABr35** was synthesized from 2-methylbenzoxazole (0.38 mL, 3.2 mmol), 3,5-dibromobenzaldehyde (0.84 g, 3.2 mmol) and *t*-BuOK (0.78 g, 7.0mmol). The crude product was purified by column chromatography (silica gel) using ethyl acetate/petroleum ether (v/v = 1/10) as the eluent. Flocculus-like white solid of **BOABr35** (0.61 g) was obtained in a yield of 50%. Mp: 191.0-192.0°C. ^{1}H NMR (400 MHz, DMSO-d_6) δ (ppm): 8.13 (s, 2H), 7.87 (s, 1H), 7.80 (d, *J* = 6.4 Hz, 1H), 7.77 (s, 1H), 7.74 (s, 1H), 7.55 (d, *J* = 16.4 Hz, 1H), 7.46-7.39 (m, 2H) (Figure S28). ^{13}C NMR (101 MHz, DMSO-d_6) δ (ppm): 162.23 (s), 150.29 (s), 142.07 (s), 139.61 (s), 136.82 (s), 134.53 (s), 130.03 (s), 126.38 (s), 125.38 (s), 123.53 (s), 120.34 (s), 117.46 (s), 111.17 (s) (Figure S29). HRMS, m/z: calc.: 379.9104, found: 379.9104 (Figure S30). FT-IR (KBr, cm^{-1}): 1602, 1385, 1166, 1073, 948, 859, 741, 547, 518.

(E)-2-(2,4-difluorostyryl)benzo[d]thiazole (BTAF24)

By following the synthetic procedure for compound **BOAF4**, **BTAF24** was synthesized from 2-methylbenzothiazole (0.41 mL, 3.2 mmol), 2,4-difluorobenzaldehyde (0.45 g, 3.2 mmol) and *t*-BuOK (0.78 g, 7.0mmol). The crude product was purified by column chromatography (silica gel) using ethyl acetate/petroleum ether (v/v = 1/10) as the eluent. Flocculus-like white solid of **BTAF24** (0.37 g) was obtained in a yield of 42%. ^{1}H NMR (400 MHz, DMSO-d_6) δ (ppm): 8.11 (d, *J* = 7.9 Hz, 1H), 8.03 (dd, *J* = 19.9, 8.3 Hz, 2H), 7.66 (s, 2H), 7.54 (t, *J* = 7.6 Hz, 1H), 7.46 (t, *J* = 7.5 Hz, 1H), 7.39 (t, *J* = 10.2 Hz, 1H), 7.22 (t, *J* = 8.3 Hz, 1H) (Figure S31). ^{13}C NMR (101 MHz, DMSO-d_6) δ (ppm): 166.36 (s), 153.84 (s), 134.62 (s), 130.65 (s), 128.42 (s), 127.12 (s), 126.12 (s), 124.44 (s), 123.20 (s), 122.73 (s), 120.19 (s), 112.99 (d, *J* = 21.1 Hz), 105.08 (t, *J* = 26.2 Hz) (Figure S32). HRMS, m/z: calc.: 274.0497, found: 274.0508 (Figure S33). FT-IR (KBr, cm^{-1}): 2026, 1605, 1285, 1163, 1074, 952, 860, 547, 523.

(E)-2-(2,4-dichlorostyryl)benzo[d]thiazole (BTACl24)

By following the synthetic procedure for compound **BOAF4**, **BTACl24** was synthesized from 2-methylbenzothiazole (0.41 mL, 3.2 mmol), 2,4-dicholorobenzaldehyde (0.56 g, 3.2 mmol) and *t*-BuOK (0.78 g, 7.0mmol). The crude product was purified by column chromatography (silica gel) using ethyl acetate/petroleum ether (v/v = 1/10) as the eluent. Flocculus-like white solid of **BTACl24** (0.77 g) was obtained in a yield of 80%. ^{1}H NMR (400 MHz, DMSO-d_6) δ (ppm): 8.13 (d, *J* = 7.9 Hz, 1H), 8.10 (d, *J* = 8.6 Hz, 1H), 8.04 (d, *J* = 8.0 Hz, 1H), 7.87 (d, *J* = 16.1 Hz, 1H), 7.76 (dd, *J* = 9.1, *J*= 7.0 Hz, 2H), 7.54 (ddd, *J* = 7.0, *J*= 5.6, *J*= 4.7 Hz, 2H), 7.47 (t, *J* = 7.3 Hz, 1H) (Figure S34). ^{13}C NMR (101 MHz, $CDCl_3$) δ (ppm): 135.48 (s), 134.74 (s), 132.37 (s), 132.13 (s), 129.96 (s), 127.73 (d, J = 6.6 Hz), 126.56 (s), 125.82 (s), 124.86 (s), 123.18 (s), 121.62 (s) (Figure S35). HRMS, m/z: calc.: 305.9906, found: 305.9905 (Figure S36). FT-IR (KBr, cm^{-1}): 2025, 1604, 1385, 1163, 1075, 946, 860, 546, 523.

(E)-2-(2,4-dibromostyryl)benzo[d]thiazole (BTABr24)

By following the synthetic procedure for compound **BOAF4**, **BTABr24** was synthesized from 2-methylbenzothiazole (0.41 mL, 3.2 mmol), 2,4-dibromobenzaldehyde (0.84 g, 3.2 mmol) and *t*-BuOK (0.78 g, 76 mmol). The crude product was purified by column chromatography (silica gel) using ethyl acetate/petroleum ether (v/v = 1/10) as the eluent. Flocculus-

like white solid of **BTABr24** (0.67 g) was obtained in a yield of 53%. ^{1}H NMR (400 MHz, DMSO-d_6) δ (ppm): 8.13 (d, *J* = 7.9 Hz, 1H), 8.05 (d, *J* = 8.1 Hz, 1H), 8.00 (d, *J* = 9.3 Hz, 2H), 7.84 (d, *J* = 16.0 Hz, 1H), 7.74 (d, *J* = 16.2 Hz, 1H), 7.69 (d, *J* = 8.6 Hz, 1H), 7.55 (t, *J* = 7.6 Hz, 1H), 7.48 (t, *J* = 7.5 Hz, 1H) (Figure S37). ^{13}C NMR (101 MHz, DMSO-d_6) δ (ppm): 165.83 (s), 153.90 (s), 135.87-135.64 (m), 135.16 (d, *J* = 78.1 Hz), 134.26 (s), 133.66 (s), 131.80 (s), 129.66 (s), 127.24 (s), 126.25 (s), 125.63 (s), 125.24 (s), 123.45 (d, *J* = 17.3 Hz), 122.82 (s) (Figure S38). HRMS, m/z: calc.: 395.8875, found: 395.8886 (Figure S39). FT-IR (KBr, cm^{-1}): 2025, 1604, 1385, 1163, 1074, 946, 860, 547, 523.

Conflicts of interest

There are no conflicts of interest to declare.

Acknowledgements

This work was financially supported by the National Natural Science Foundation of China (51773076 and 21503090) and the Open Project of State Key Laboratory of Supramolecular Structure and Materials SKLSSM201813).

Notes and references

1. (a) P. Terech and R. G. Weiss, *Chem. Rev.*, 1997, **97**, 3133-3160; (b) M. Muccini, *Nat. Mater.*, 2006, **5**, 605-613; (c) C. Vijayakumar, V. K. Praveen and A. Ajayaghosh, *Adv. Mater.*, 2010, **21**, 2059-2063; (d) M. Mas-Torrent and C. Rovira, *Chem. Rev.*, 2011, **111**, 4833-4856; (e) X. Yu, L. Chen, M. Zhang and T. Yi, *Chem. Soc. Rev.*, 2014, **43**, 5346-5371; (f) J. Puig, I. E. D. Erba, W. F. Schroeder, C. E. Hoppe and R. J. J. Williams, *ACS Appl. Mater. Interfaces*, 2017, **9**, 11126-11133.
2. (a) S. S. Babu, S. Prasanthkumar and A. Ajayaghosh, *Angew. Chem. Int. Ed.*, 2012, **51**, 1766-1776; (b) K. Ghosh, D. Kar, S. Panja and S. Bhattacharya, *RSC Adv.*, 2013, **4**, 3798-3803; (c) N. Yan, Z. Xu, K. K. Diehn, S. R. Raghavan, Y. Fang and R. G. Weiss, *J. Am. Chem. Soc.*, 2013, **135**, 8989-8999; (d) Z. Zhao, J. W. Y. Lam and B. Z. Tang, *Soft Matter*, 2013, **9**, 4564-4579; (e) X. Li, Y. Zhang, A. Chen, B. Zhang, B. Zhang and J. Song, *RSC Adv.*, 2017, **7**, 37105-37111.
3. (a) S. Diring, F. Camerel, B. Donnio, T. Dintzer, S. Toffanin, R. Capelli, M. Muccini and R. Ziessel, *J. Am. Chem. Soc.*, 2009, **131**, 18177-18185; (b) J. P. Hong, M. C. Um, S. R. Nam, J. I. Hong and S. Lee, *Chem. Commun.*, 2009, **3**, 310-312; (c) W. W. Tsai, I. D. Tevis, A. S. Tayi, H. Cui and S. I. Stupp, *J. Phys. Chem. B*, 2010, **114**, 14778-14786; (d) D. A. Stone, A. S. Tayi, J. E. Goldberger, L. C. Palmer and S. I. Stupp, *Chem. Commun.*, 2011, **47**, 5702-5704; (e) Y. Ge, C. A. Di, G. Zhang, Z. Jing, J. Xiang, D. Zhang and D. Zhu, *Adv. Funct. Mater.*, 2013, **23**, 1671-1676; (f) R. Marty, R. Nigon, D. Leite and H. Frauenrath, *J. Am. Chem. Soc.*, 2014, **136**, 3919-3927; (g) Y. S. Guan, Y. Qin, Y. Sun, C. Wang, W. Xu and D. Zhu, *Chem. Commun.*, 2015, **51**, 12182-12184; (h) L. Fang, Y. Hu, Q. Li, S. Xu, M. K. Dhinakarank, W. Gong and G. Ning, *Org. Biomol. Chem*, 2016, **14**, 4039-4045; (i) T. Ikeda, T. Masuda, M. Takayama, H. Adachi and T. Haino, *Org. Biomol. Chem*, 2016, **14**, 36-39; (j) H. Mehdi, H. Pang, W. Gong, M. K. Dhinakaran, A. Wajahat, X. Kuang and G. Ning, *Org. Biomol. Chem.*, 2016, **14**, 5956-5964; (k) X. Pang, X. Yu, D. Xie, Y. Li, L. Geng, J. Ren and X. Zhen, *Org. Biomol. Chem.*, 2016, **14**, 11176-11182; (l) J. Xu, Y. Wang, H. Shan, Y. Lin, Q. Chen, V. A. Roy and Z. Xu, *ACS Appl. Mater. Interfaces*, 2016, **8**, 18991-18997.
4. (a) Y. Li, K. Liu, J. Liu, J. Peng, A. Xuli Feng and Y. Fang, *Langmuir*, 2006, **22**, 7016-7020; (b) L. E. Buerkle and S. J. Rowan, *Chem. Soc. Rev.*, 2012, **41**, 6089-6102; (c) H. Peng, D. L. Ding, T. Liu, X. Chen, L. Li, D. S. Yin and D. Y. Fang, *Chem. Asian J.*, 2012, **7**, 1576-1582.
5. (a) K. Sugiyasu, N. Fujita, M. Takeuchi, S. Yamada and S. Shinkai, *Org. Biomol. Chem.*, 2003, **1**, 895-899; (b) X. Wang, P. Duan and M. Liu, *Chem. Commun.*, 2012, **48**, 7501-7503; (c) X. Cao, A. Gao, H. Lv, Y. Wu, X. Wang and Y. Fan, *Org. Biomol. Chem.*, 2013, **11**, 7931-7937; (d) P. Xue, J. Sun, Q. Xu, R. Lu, M. Takafuji and H. Ihara, *Org. Biomol. Chem.*, 2013, **11**, 1840-1847; (e) G. Qing, X. Shan, W. Chen, Z. Lv, P. Xiong and T. Sun, *Angew. Chem. Int. Ed.*, 2014, **53**, 2124-2129; (f) D. F. Xu, X. L. Liu, R. Lu, P. C. Xue, X. F. Zhang, H. P. Zhou and J. H. Jia, *Org. Biomol. Chem.*, 2011, **9**, 1523-1528.
6. (a) S. Bhattacharya and S. K. Samanta, *Langmuir*, 2009, **25**, 8378-8381; (b) H. Jintoku, M. Takafuji, R. Oda and H. Ihara, *Chem. Commun.*, 2012, **48**, 4881-4883.
7. J. Lee, E. K. Ji, Y. You and S. Y. Park, *Langmuir*, 2014, **30**, 2842-2851.
8. (a) Y. Feng, Y. He and Q. Fan, *Chem. Asian J.*, 2014, **9**, 1724-1750; (b) Y. Feng, Z. T. Liu, J. Liu, Y. M. He, Q. Y. Zheng and Q. H. Fan, *J. Am. Chem. Soc.*, 2009, **131**, 7950-7951; (c) Q. Chen, Y. Feng, D. Zhang, G. Zhang, Q. Fan, S. Sun and D. Zhu, *Adv. Funct. Mater.*, 2010, **20**, 36-42.
9. Z. Xie, V. Stepanenko, B. Fimmel and F. Wurthner, *Mater. Horiz.*, 2014, **1**, 355-359.
10. (a) X. Yang, R. Lu, T. Xu, P. Xue, X. Liu and Y. Zhao, *Chem. Commun.*, 2008, **8**, 453-455; (b) X. Yang, R. Lu, F. Gai, P. Xue and Y. Zhan, *Chem. Commun.*, 2010, **46**, 1088-1090; (c) J. Sun, P. C. Xue, J. Sun, P. Gong, P. Wang and R. Lu, *J. Mater. Chem. C*, 2015, **3**, 8888-8894; (d) J. Sun, J. Sun, W. Mi, P. Xue, J. Zhao, L. Zhai and R. Lu, *Dyes Pigments*, 2017, **136**, 633-640.
11. (a) P. Gong, H. Yang, J. Sun, Z. Zhang, J. Sun, P. Xue and R. Lu, *J. Mater. Chem. C*, 2015, **3**, 10302-10308; (b) J. Sun, J. Sun, W. Mi, P. Xue, J. Zhao, L. Zhai and R. Lu, *New J. Chem.*, 2016, **41**, 763-772; (c) L. Zhai, M. Liu, P. Xue, J. Sun, P. Gong, Z. Zhang, J. Sun and R. Lu, *J. Mater. Chem. C*, 2016, **4**, 7939-7947; (d) L. Zhai, F. Zhang, J. Sun, M. Liu, M. Sun and R. Lu, *Dyes Pigments*, 2017, **145**, 54-62.
12. P. Xue, B. Yao, P. Wang, J. Sun, Z. Zhang and R. Lu, *RSC Adv.*, 2014, **4**, 61548-61548.
13. Z. Wu, J. Sun, Z. Zhang, H. Yang, P. Xue and R. Lu, *Chem. Eur. J.*, 2017, **23**, 1901-1909.
14. H. Wang, P. Chen, Z. Wu, J. Zhao, J. Sun and R. Lu, *Angew. Chem. Int. Ed.*, 2017, **56**, 9463-9467.
15. (a) H. Jintokua and H. Ihara, *Chem. Commun.*, 2012, **48**, 1144-1146; (b) H. Jintoku, M.-T. Kao, A. D. Guerzo, Y. Yoshigashima, T. Masunaga, M. Takafuji and H. Ihara, *J. Mater. Chem. C*, 2015, **3**, 5970-5975; (c) S. Mondal, P. Chakraborty, P. Bairi, D. P. Chatterjee and A. K. Nandi, *Chem. Commun.*, 2015, **51**, 10680-10683.
16. (a) K. K. Kartha, S. S. Babu, S. Srinivasan and A. Ajayaghosh, *J. Am. Chem. Soc.*, 2012, **134**, 4834-4841; (b) G. Hong, C. Qian, P. Xue, X. Liu, Q. Wang, M. Liu, P. Gong and R. Lu, *Eur. J. Org. Chem.*, 2014, 6155-6162.
17. A. Griffith, T. J. Bandy, M. Light and E. Stulz, *Chem. Commun.*, 2012, **49**, 731-733.
18. (a) P. Thordarson, *Chem. Soc. Rev.*, 2011, **40**, 1305-1323; (b) P. Vishnoi, M. G. Walawalkar, S. Sen, A. Datta, G. N. Patwari and R. Murugavel, *Phys. Chem. Chem. Phys.*, 2014, **16**, 10651-10658; (c) P. Xue, J. Sun, B. Yao, P. Gong, Z. Zhang, C. Qian, Y. Zhang and R. Lu, *Chem. Eur. J.*, 2015, **21**, 4712-4720.